

8th International Conference on Photonic Technologies LANE 2014

Layerwise Monitoring of the Selective Laser Melting Process by Thermography

Harald Krauss^{a,*}, Thomas Zeugner^b, Michael F. Zaeh^a

^a*Institute for Machine Tools and Industrial Management, Technische Universitaet Muenchen, Application Center Augsburg*

^b*Institute of Physics, University of Augsburg*

Abstract

Selective Laser Melting is utilized to build parts directly from CAD data. In this study layerwise monitoring of the temperature distribution is used to gather information about the process stability and the resulting part quality. The heat distribution varies with different kinds of parameters including scan vector length, laser power, layer thickness and inter-part distance in the job layout. By integration of an off-axis mounted uncooled thermal detector, the solidification as well as the layer deposition are monitored and evaluated. This enables the identification of hot spots in an early stage during the solidification process and helps to avoid process interrupts. Potential quality indicators are derived from spatially resolved measurement data and are correlated to the resulting part properties. A model of heat dissipation is presented based on the measurement of the material response for varying heat input. Current results show the feasibility of process surveillance by thermography for a limited section of the building platform in a commercial system.

© 2014 Published by Elsevier B.V. This is an open access article under the CC BY-NC-ND license (<http://creativecommons.org/licenses/by-nc-nd/3.0/>).

Peer-review under responsibility of the Bayerisches Laserzentrum GmbH

Keywords: Selective Laser Melting; Process Monitoring; Thermography; Part Quality; Heat Dissipation

1. Introduction

Selective Laser Melting is a heat intense process giving rise for temperature monitoring in order to detect irregularities or errors. Thin layers of metallic powder particles are selectively melted by scanning adjacent vectors with a high energy laser beam. Using CAD data only, high quality metallic components are produced by stacking individual layers. Today, process monitoring is of great importance for demanding applications and it should be feasible with a reasonable cost-benefit ratio in order to help spreading the promising technology of additive layer manufacturing (ALM). In-Process monitoring approaches can be divided into off-axis systems measuring the whole build area at a time and on-axis systems focusing on the current beam position. In Craeghs et al. (2011), Zur Jacobsmühlen et al. (2013), Kleszczynski et al. (2012) and Grünberger et al. (2013) off-axis arrangements are presented, investigating the detection of coating errors that may arise when a new layer of metallic powder is applied. Furthermore the appearance

* Corresponding author. Tel.: +49-821-568-8334 ; fax: +49-821-568-8350 .
E-mail address: harald.krauss@iwb.tum.de

of the solidified surface is checked. On-axis setups use the same scanning and focusing unit as the processing laser in order to directly monitor the melt pool and its environment (Chivel (2013); Craeghs et al. (2010, 2012); Lott et al. (2011)). The usable wavelength band for monitoring of process emissions is severely restricted to a small band close to the laser wavelength because the same optics are employed. To enable real-time process control, on-axis setups apply sampling rates in the kHz range which are significantly higher compared to off-axis systems. This allows for continuous measurement of melt pool dynamics at scanning velocities of several meters per second.

Nomenclature

K	key indicator
j	layer index
c_p	specific heat capacity
a	thermal diffusivity
l	effective melt depth
η	absorptivity
v	scan velocity
d	hatch distance
Δ	imperfection level

2. Approach and Setup

A local change in heat flow during heat-up or cool down indicates inhomogeneous material properties and potential irregularities. Given a significant thermal contrast, these irregularities can in principle be identified and characterized. The approach in this paper uses the process heat that is induced by the laser to find inhomogeneities in the current layer. It aims at measuring the temporal evolution of the temperature distribution and comparing it to a simplified model in order to identify a process beyond its boundaries. The experiments were conducted on a commercial additive manufacturing system EOS M270 using a microbolometer thermal detector mounted off-axis at the process chamber door (Krauss et al. (2012)). The manufacturing system features a 200 W Ytterbium fiber laser, a high speed galvanometer scanning unit and an f/Θ -lens focusing the laser beam onto a fixed building platform. A TEM_{00} beam having a diameter of $70\ \mu\text{m}$ and beam quality $M^2 < 1.1$ melts metallic powder particles with a mean grain size of $30\ \mu\text{m}$ on the building platform. The thermal detector aims at a view angle of 55 degrees on this platform, reaches a pixel resolution of approx. $250\ \mu\text{m}$ per pixel and operates at 50 Hz. Solidification is done using a stripe exposure strategy where adjacent hatch vectors of constant length and spacing are scanned and form a stripe of variable length depending on the part geometry. Even though the melt pool expands over a single hatch vector at maximum, the recurring energy input for adjacent scan tracks continuously reheats already solidified tracks (c.f. Figure 2). Process

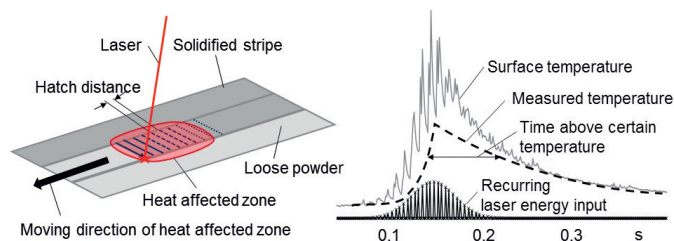


Fig. 1. (a) Stripe exposure; (b) Recurring energy input

irregularities may arise due to improper heat dissipation caused by, amongst others, varying layer thickness, foreign particles, process parameter fluctuation or drifts. However, the main contribution comes from the part geometry itself.

Overhanging or filigree structures are subjected to a reduced heat dissipation. This may cause elevated structures in the powder bed which obstruct the application of new powder layers, Yasa et al. (2009). Furthermore residual stresses may lead to delamination issues or part bending during the process, causing coating problems as well.

3. Layerwise Data Acquisition and Processing

In order to gather quality information for every single layer that is solidified, a layerwise monitoring approach is presented. It is based on the mapping of process data to the 2D position space corresponding to the build level. The off-axis monitoring system and suitable data processing algorithms are utilized to derive spatially resolved key indicators. The input data for these key indicators is based on the time-resolved temperature measurements during the full processing ($t_{j\text{start}}, \dots, t_{j\text{end}}$) of the layer under question (c.f. equation 1).

$$\vec{K}(x_0, y_0)_j = \vec{f}(T(x, y, [t_{j\text{start}}, \dots, t_{j\text{end}}])) \quad (1)$$

Existing approaches for information condensation and visualization in the field of additive manufacturing process monitoring are based on coaxial setups (Craeghs et al. (2012)). Since mapping is conducted on the basis of the current scan position, the measurement value is recorded at a single time and location only, $\vec{K}(x_0, y_0)_j = \vec{f}(T(x_0, y_0, t_0))$. Using off-axis setups, the entire temporal evolution of the current layer data can be characterized. The objective is to find key indicators that maximize the correlation to the part quality for example in terms of porosity, hardness, residual stress or deformation. As proposed in Krauss et al. (2014) different types of key indicators exist which have to be checked for their relevance. Examples are maximum temperature, cool-down behavior in terms of a characteristic time τ_c and heat flow in terms of a time above a certain threshold t_{above} or an effective heat conductivity a_{eff} focused in this work. The mapping approach is not restricted to measurement data collected from the location under question. The function \vec{f} for deriving key indicators generally acts on the complete data set which corresponds to all captured frames of the considered layer. This can be of particular interest for mapping geometrical features of the processing zone or sputter activity that may extend over a large area. Key indicators are assigned to every location¹ of the current cross section for the entire layer. This layerwise approach allows for a quality report consisting of one image per key indicator and layer. Through stacking of individual layer data, as known from tomography, a three dimensional quality report for key indicators can be generated (c.f. Figure 2).

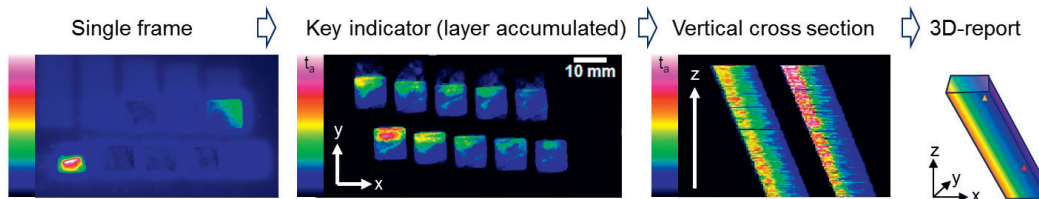


Fig. 2. Data processing to generate a visual quality report.

4. Model of Heat Dissipation

During melting the applied laser energy is transformed into process heat. Neglecting radiation and convection losses, the process heat is dissipated by heat conduction through solidified portions of the component being built. Since loose powder has a thermal conductivity approx. 100 times smaller than solidified material (Rombouts et al. (2005)), it has practically no contribution to the heat conduction. The presented model assumes heat conduction to occur predominantly in the vertical direction because of the existing thermal gradient pointing at the build platform

¹ The averaging area depends on the pixel resolution of the detection system.

in the negative build direction. For further simplification no phase transitions are taken into account² and the specific heat capacity c_p and thermal diffusivity a_{eff} are assumed to be independent of the temperature. The situation directly after solidification ($t = t_0$, temperature already below solidus) is modeled as a semi infinite bar having a constant temperature of $T = T_0$ for $z \in]-\infty, -l]$ and a temperature of $T = T_1 > T_0$ in a small volume of height l at its end. The thickness l corresponds to an effective melt depth, where the applied energy is assumed to be completely absorbed directly after the laser beam passes by. The thermal isolation at the bar's top end is modeled through mirroring (Krauss et al. (2014)). The initial condition $T(z, t_0)$ can be summarized as follows (Θ being the Heaviside function):

$$T(z, t_0) = T_0 + (T_1 - T_0)(\Theta(z + l) - \Theta(z - l)) = \begin{cases} T_0 : & z < -l \\ T_1 : & -l \geq z \geq l \\ T_0 : & z > l \end{cases} \quad (2)$$

Using the fundamental solution to the heat conduction equation given by equation 3, the surface temperature $T_s(t)$ is given by equation 4.

$$U(x, t) = \frac{1}{\sqrt{4\pi at}} e^{-\frac{x^2}{4at}} \quad (3)$$

$$T_s(t) = T_0 + (T_1 - T_0) \operatorname{erf}\left(\frac{l}{\sqrt{4at}}\right) \quad (4)$$

The temperature rise $T_d = T_1 - T_0$ after heat input can be estimated by evaluating the energy input E as follows (η being the absorptivity):

$$\begin{aligned} E &= T_d c_p m \\ &= T_d c_p \rho A l \\ &= \eta P t_A \end{aligned} \quad (5)$$

The time t_A for exposing area A is given by $A = v t_A d$ and the temperature rise T_d can be described in terms of power input per area:

$$\begin{aligned} \eta P \frac{A}{vd} &= T_d c_p \rho A l \\ \rightarrow T_d &= \frac{\eta P}{v d c_p \rho l} \end{aligned} \quad (6)$$

The model assumes that the energy is homogeneously applied to the surface element of interest. For verification purposes a surface element has to be chosen that is either much smaller than the laser beam diameter or several adjacent scan vectors have to be scanned on the same surface element in a comparatively short time.

5. Results and discussion

For the purpose of model verification a set of 13 rectangular-shaped density specimens was investigated by measuring the surface temperature during build-up and deriving an effective thermal diffusivity a_{eff} . Through approximation of a_{eff} by series expansion of equation 4 and neglecting higher order terms, the effective thermal diffusivity becomes independent of the melt volume depth l (c.f. equation 7).

$$\begin{aligned} T(t) &\approx T_0 + \frac{\eta}{\sqrt{t}} \frac{P}{V d c_p \rho \sqrt{\pi a}} \\ \Leftrightarrow a &\approx \frac{1}{t} \left(\frac{1}{T(t) - T_0} \right)^2 \left(\frac{P \eta}{V d c_p \rho \sqrt{\pi}} \right)^2 \end{aligned} \quad (7)$$

Heat conduction through the specimens was varied by changing the laser power P and scan velocity v . After a build height of $z_0 = 5.7$ mm all samples were exposed with equal standard parameters known to generate fully dense parts.

² temperatures are only measured after melt is solidified due to measurement system inertia

This approach produces pores and binding errors within the lower part of the specimens and leads to a deterioration of thermal conductivity depending on the amount of imperfections. Figure 3 (left) shows the measured temperature evolution of one layer after exposure compared to the theoretical behavior according to equation 7. Model parameters were chosen according to the processing parameters P and ν , η is assumed to be 60% and thermal diffusivity $a = 4.36 \times 10^{-6} \text{ m}^2/\text{s}$ is given in Sweet et al. (1987). The model corresponds to the measured temperature evolution, but a temporal offset in the order of 100 ms has to be taken into account. This is potentially due to the fact, that heat input is finished not directly after exposure of the area under question. The solidification of neighboring elements causes a slight reheating and cool down delay. Furthermore, the characteristic detector response time in the order of milliseconds causes an additional delay.

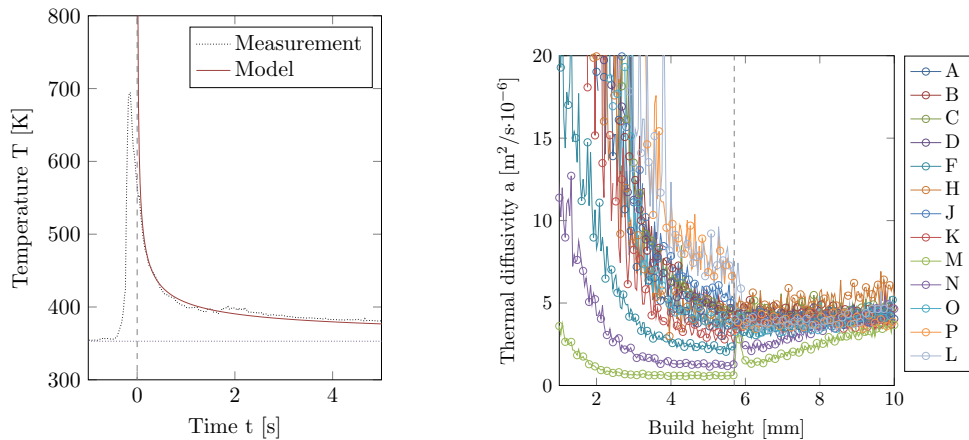


Fig. 3. (a) Measured temperature evolution after exposure compared to model. (b) Derived effective thermal diffusivity a_{eff} averaged by layer over the part cross section versus build height. The thermal diffusivity is averaged between 0.5 ... 5 s to account for measurement errors concerning peak temperature determination and small temperature differences at long times after exposure.

Using the sample specific P and ν values, Figure 3 (right) shows the derived thermal diffusivity a_{eff} according to equation 7, averaged by layer over the complete specimen cross section versus build height. It can be seen that thermal diffusivity decreases significantly for build height $z = 0 \dots 4 \text{ mm}$. This is explained by the reduced thermal influence of the build platform with increasing build height. At small build heights the build platform's heat capacity and the short distance to the current layer lead to a fast cool down corresponding to a high effective thermal diffusivity a_{eff} .

The absolute difference in thermal diffusivity for build heights smaller than z_0 is a result of two effects:

1. Porosity and binding errors due to the chosen processing parameters cause a reduced thermal conductivity.
2. Temperature measurement is based on surface emissivity properties. Since surface properties vary with processing parameters, the emissivity varies as well and causes different measured temperature values for different specimens. According to equation 7 this leads to a change in the derived thermal diffusivity. The start temperature T_0 is measured after application of a new powder layer and is not affected by surface properties of the melted sample whereas the measurement of the current temperature $T(t)$ is influenced by the surface properties.

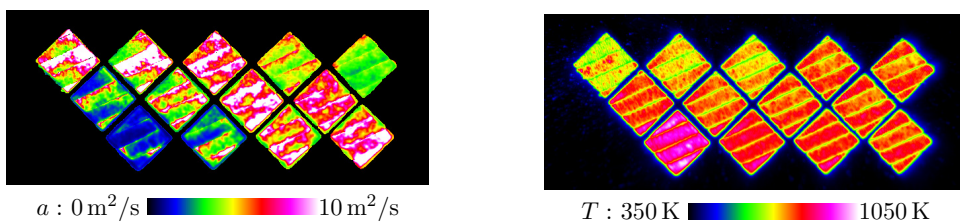


Fig. 4. Mapped key indicators for build height 3.6 mm: thermal diffusivity (left) and maximum measured temperature (right)

Regarding the layerwise evaluation of derived key indicators, different process parameters or drifts can be visually identified (c.f. Figure 4). The significant variation of surface properties across individual samples is due to the chosen exposure strategy. On the one hand this enables the detection of surface irregularities, on the other hand it will affect the fluctuation when considering averaged key indicators (i.e. thermal diffusivity per part per layer). The fluctuation of thermal diffusivity is in the order of approx. $2 \times 10^{-6} \text{ m}^2/\text{s}$ and is caused by the averaging approach in the following way. Data is gathered by pixel-wise calculation of thermal diffusivity and spatial averaging over the specimen's cross section. However, this cross section has different surface properties depending on the direction of the solidified stripes (c.f. Figure 4) and features different thermal behavior at its edge regions due to the changing scan vector length going along with an exposure specific rotating stripe direction.

The difference in thermal diffusivity caused by surface effects and material properties ($z < z_0$) can be correlated to the resulting part quality. Figure 5 (right) shows the imperfection level Δ in terms of porosity and binding errors and the thermal diffusivity for the investigated samples. Depending on the different energy input for each sample a change in the imperfection level can be identified ($(P, v) \leftrightarrow \Delta$). The calculated correlation coefficients for the parameters in question are summarized in Table 1. Delaminated samples feature comparably low thermal diffusivities (sample M, N) and high imperfection levels which make them easy to detect. For dense parts without delamination issues the thermal diffusivity is significantly higher. Considering the inadequacies in determining an absolute value for thermal diffusivity the unambiguous distinction between different energy inputs or imperfection levels remains a challenging task. In principle, however, the considered key indicator is suitable for detecting high imperfection levels, or strongly varying energy inputs since the correlation coefficient is in the order of 0.7. Because of the limited spatial and temporal resolution of the measurement equipment as well as the boundary conditions for thermographic measurements regarding changing surface properties and changing ambient temperatures, the detection limit for this key indicator has to be further analyzed.

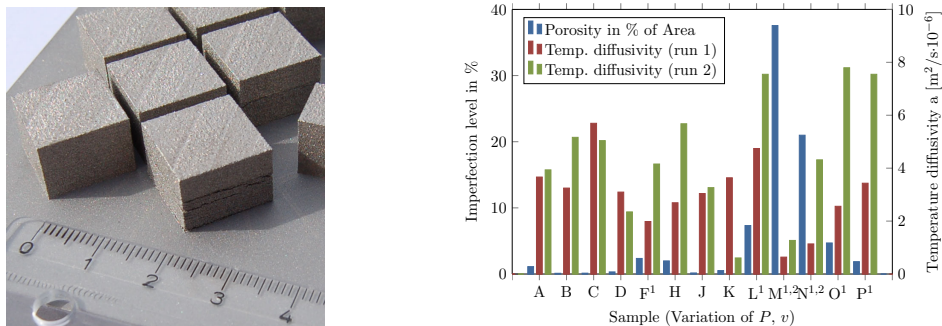


Fig. 5. Delamination of test specimens (left), Imperfection level and measured thermal diffusivity at build height 4 mm averaged over five subsequent layers (right).

Table 1. Correlation coefficients for investigated specimens for a selected layer at build height 4 mm. Delamination is subjectively characterized by its severeness.

	Energy input P/v	Imperfection level Δ	Delamination (a.u.)	Thermal diffusivity a_{eff}
Energy input P/v	1			
Imperfection level Δ	-0.6	1		
Delamination (a.u.)	-0.7	0.9	1	
Thermal diffusivity a_{eff}	0.6	-0.7	-0.8	1

After applying standard parameters to all specimens $z > z_0$ (c.f. Figure 3) the effect of different surface properties becomes negligible and the thermal properties of the specimens are expected to be homogenized. The difference

in thermal diffusivity for samples L,M,N,O,P therefore can only be caused by material properties or geometrical properties underneath the current layer that influence the heat conductivity. In this regard, delamination issues (c.f. Figure 5) were found to have a major contribution. The investigations show, that these kinds of errors can in principle be detected at comparatively long distances.

6. Conclusion and Outlook

Regarding accumulated data by layer, thermographic measurements in terms of effective thermal diffusivity can reveal changing or incorrect exposure parameters as well as irregularities in a straight forward manner. Inner material defects (small errors) can be detected by investigating layers close to the zone of irregularities. Additionally, delaminations (big errors) can also be detected at great distances to the erroneous inter-layer connection. By averaging over a specimen's cross section, different surface properties caused by the exposure strategy contribute to the fluctuations which in turn complicate the correlation of the highly compacted measurement data to the part quality. From this point of view, the measurement accuracy and the presented averaging approach have to be improved in future work. The presented work however shows, that inferior part quality (high imperfection level, delamination) in underlying layers can be detected even though the same exposure parameters are applied at the current layer. Since the difference in thermal diffusivity will become less for increasing distance to the irregularities the detectability will vanish at some point.

The model for thermal diffusivity given above neglects the recurring energy input characteristic of the exposing strategy. Taking this into account would require that the material response $T_{mat}(t)$ to a single hatch vector is known. Then the repeated energy input can be modeled by using a mean temperature rise \bar{T} depending on the amount of passes and temporal distance between subsequent passes of the laser beam. Once the laser beam is outside of the sphere of influence, the heat conduction can then be assumed to be given by equation 4, but with temperature difference \bar{T} . The detailed investigation on the material response is the topic of ongoing research employing high speed and high resolution temperature measurements.

Furthermore, it has to be noted, that the given model is valid only if the melt volume depth is high enough to establish a thermal contact to the solidified volume (heat conduction primarily in the z direction). When the melt volume depth is too low, the thermal contact becomes insufficient and the model assumptions become invalid because heat transport takes place in all directions and not only in the build direction.

Acknowledgements

The IGF-Project No 17.911 N / DVS-No. 13.007 of the Research Association, Schweißen und verwandte Verfahren e.V. des DVS, Aachener Str. 172, 40223 Düsseldorf, was promoted by the AiF under the program for the promotion of industrial research and development (IGF) by the Federal Ministry of Economics and Technology based on a decision by the German Bundestag. Infratec GmbH as a supplier of thermography equipment is acknowledged for fruitful discussions.

References

- Chivel, Y., 2013. Optical in-process temperature monitoring of selective laser melting. *Physics Procedia* 41, 904–910. doi:10.1016/j.phpro.2013.03.165.
- Craeghs, T., Bechmann, F., Berumen, S., Kruth, J.P., 2010. Feedback control of layerwise laser melting using optical sensors. *Physics Procedia* 5, 505–514. doi:10.1016/j.phpro.2010.08.078.
- Craeghs, T., Clijsters, S., Kruth, J.P., Bechmann, F., Ebert, M.C., 2012. Detection of process failures in layerwise laser melting with optical process monitoring. *Physics Procedia* 39, 753–759. doi:10.1016/j.phpro.2012.10.097.
- Craeghs, T., Clijsters, S., Yasa, E., Kruth, J.P., 2011. Online quality control of selective laser melting, in: Bourell, D. (Ed.), *Solid Freeform Fabrication: Proceedings*, August 2011, University of Texas at Austin.
- Grünberger, T., Wöber, W., Seemann, R., 2013. Optische prozessüberwachung bei selektiven laserschmelzverfahren, in: *Messe Erfurt (Ed.), Rapid.Tech 2013 - Fachmesse und Anwendertagung für Rapid-Technologie*.
- Kleszczynski, S., zur Jacobsmühlen, J., Sehart, J.T., Witt, G., 2012. Error detection in laser beam melting systems by high resolution imaging, in: Bourell, D. (Ed.), *Solid Freeform Fabrication: Proceedings*, August 2012, University of Texas at Austin.

- Krauss, H., Eschey, C., Zäh, M.F., 2012. Thermography for monitoring the selective laser melting process, in: Bourell, D. (Ed.), Solid Freeform Fabrication: Proceedings, August 2012, University of Texas at Austin.
- Krauss, H., Zeugner, T., Zäh, M.F., 2014. Detecting process irregularities in selective laser melting by thermography, in: Fraunhofer Additive Manufacturing Alliance (Ed.), Fraunhofer Direct Digital Manufacturing Conference 2014.
- Lott, P., Schleifenbaum, H., Meiners, W., Wissenbach, K., Hinke, C., Bültmann, J., 2011. Design of an optical system for the in situ process monitoring of selective laser melting (slm). *Physics Procedia* 12, 683–690. doi:10.1016/j.phpro.2011.03.085.
- Rombouts, M., Froyen, L., Gusarov, A.V., Bentefour, E.H., Glorieux, C., 2005. Photopyroelectric measurement of thermal conductivity of metallic powders. *Journal of Applied Physics* 97, 024905. doi:10.1063/1.1832740.
- Sweet, J.N., Roth, E.P., Moss, M., 1987. Thermal conductivity of inconel 718 and 304 stainless steel. *International Journal of Thermophysics* 8, 593–606. doi:10.1007/BF00503645.
- Yasa, E., Craeghs, T., Badrossamay, M., Kruth, J.P., 2009. Investigation on occurrence of elevated edges in selective laser melting, in: Bourell, D. (Ed.), Solid Freeform Fabrication: Proceedings, August 2009. University of Texas at Austin.
- Zur Jacobsmühlen, J., Kleszczynski, S., Schneider, D., Witt, G., 2013. High resolution imaging for inspection of laser beam melting systems, in: Instrumentation and Measurement Technology Conference (I2MTC), 2013 IEEE International, pp. 707–712.